Conformational Effects on Glycine Ionization Energies and Dyson Orbitals

Bárbara Herrera,[†] O. Dolgounitcheva,[‡] V. G. Zakrzewski,[‡] Alejandro Toro-Labbé,[†] and J. V. Ortiz*[,‡]

Laboratorio de Química Teórica Computacional, Facultad de Química, Pontificia Universidad Católica de Chile, Casilla 306, Correo 22, Santiago, Chile, and Department of Chemistry, Kansas State University, Manhattan, Kansas 66506-3701

Received: April 22, 2004

Five conformational isomers corresponding to minima in potential energy surfaces calculated with the B3LYP/6-311G** and MP2/6-311G** models lie within 6 kcal/mol of each other. The vertical ionization energies of the most stable isomer calculated with ab initio electron propagator theory in the P3/6-311G** approximation are in excellent agreement with experimental data from photoelectron spectroscopy. The chief components of the first four Dyson orbitals are a N lone pair, an O lone pair, π_{CO}, and C−H lobes, respectively. Conformationally induced shifts of the vertical ionization energies are explained in terms of electrostatic and phase relationships in the Dyson orbitals.

1. Introduction

Protein force fields represent the energetic consequences of bond rotations and other conformational changes in ground-state potential energy surfaces.[1] The electronic structures of these states may be described approximately in terms of a single configuration of localized electron pairs or a small number of resonance forms where there are π-conjugated fragments. In contrast, cations and anions of proteins and their amino acid constituents require the examination of delocalized, one-electron states.[2] Corresponding electron binding energies provide estimates of many useful descriptors of chemical reactivity in the finite difference approximation. For example, the chemical potential characterizes electronic charge transfer in chemical reactions, while the molecular hardness provides a measure of resistance to such fluctuations.

Glycine is the simplest amino acid and is an obvious place to begin a study of the electronic structure of polypeptides. He I photoelectron spectra on gas-phase glycine[3,4] were reported in the 1970s. Improved experiments with synchrotron radiation sources for alanine (which differs from glycine by the substitution of a methyl group for a hydrogen atom) were successfully interpreted in terms of a single conformer with the aid of electron propagator calculations.[5] In anticipation of similar investigations on other amino acids, ab initio electronic structure calculations on the ground-state minima of glycine, their relative energies, and their vertical ionization energies are reported here. Dyson orbitals, which describe changes in electronic structure between neutral and cationic states,[6,7] are analyzed and compared. Predicted differences between the ionization energies of conformers with similar energies may aid in the assignment of spectra with higher resolution and lower sample temperatures.

2. Methods

All calculations were executed with Gaussian 98[8] and Gaussian 99.[9] Preliminary geometry optimizations on various rotational isomers were performed with the B3LYP/6-311G** model.[10,11] The five local minima obtained thus were reoptimized at the MP2 level using the same basis set and were confirmed as local minima by evaluation of harmonic frequencies.

Vertical ionization energies of each rotamer were evaluated in the P3 approximation[12,13] of electron propagator theory[6,7] with the 6-311G** basis set.[11] Electron correlation and orbital relaxation effects are included in the P3 approximation. For each vertical ionization energy calculated with electron propagator methods, there corresponds a Dyson orbital defined by

$$\phi^{\mathrm{Dyson}}(x_1) = N^{-1/2}\int \Psi^{*}_{\mathrm{cation}}(x_2, x_3, x_4, \ldots, x_N) \times \Psi_{\mathrm{molecule}}(x_1, x_2, x_3, \ldots, x_N)\, \mathrm{d}x_2\, \mathrm{d}x_3\, \mathrm{d}x_4 \ldots \mathrm{d}x_N$$

where N is the number of electrons in the molecule and x_i is the space-spin coordinate of electron i. A Dyson orbital represents the change in electronic structure accompanying the detachment of an electron from a molecule. Dyson orbitals corresponding to each ionization energy in the P3 approximation are proportional to canonical, Hartree−Fock orbitals. Pole strengths, which are equal to the integral over all space of the absolute value squared of the Dyson orbital, are indices of the validity of perturbative electron propagator improvements to the results of Koopmans's theorem. When pole strengths lie between 0.85 and unity, these approximations are validated.

All figures were produced by the MOLDEN graphics program.[14] The contour values represented in the orbital plots are equal to ±0.05.

3. Results and Discussion

3.1. Structures. Many rotational isomers were considered as the initial states in the geometry optimizations. (Spectroscopic studies[15] and basicity measurements[16] established that the glycine molecule is not a zwitterion in the gas phase.) Figures 1 and 2 show the five local minima with C_s and C_1 point groups, respectively, that were verified by harmonic frequency calculations. C_1-O_1, C_1-O_2, and C_2-N bond lengths are somewhat

* Corresponding author. E-mail: ortiz@ksu.edu.
[†] Pontificia Universidad Católica de Chile.
[‡] Kansas State University.

10.1021/jp040307a CCC: $27.50
Published on Web 12/07/2004

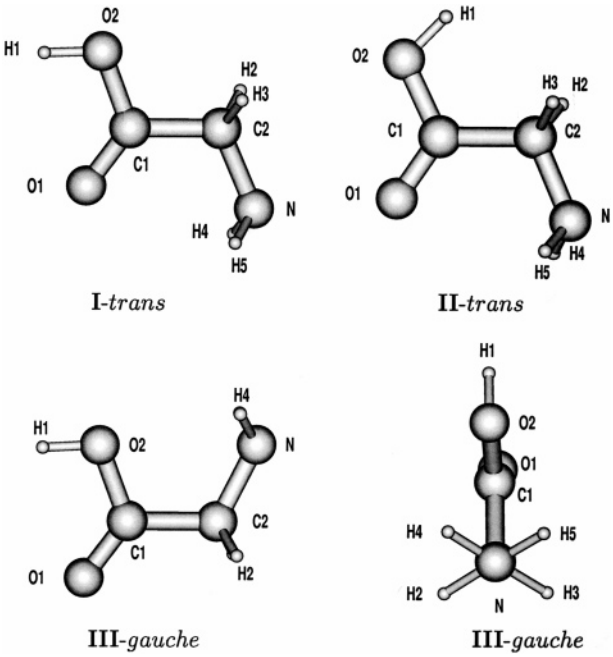

Figure 1. C_s minima: structure I, structure II, and structure III (two views).

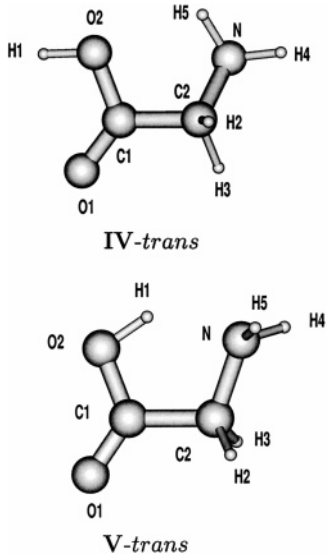

Figure 2. C_1 minima: structure IV and structure V.

shorter in the MP2 geometries; the corresponding data are given in Tables 1 and 2.

Structures I and II of Figure 1 differ in the orientation of the O−H bond with respect to the carbonyl group. The amine N is cis with respect to the carbonyl O in both cases. In the remaining three structures, there is a trans relationship between the same pair of atoms. A second view of structure III in Figure 1 exhibits the dihedral angles pertaining to C−H, N−H, and O−H bonds. The dihedral angles between N−H and C−H bonds that are gauche with respect to each other are ∼65° in all three C_s minima.

In the structures of Figure 2, the planarity of the COOH group is approximately conserved. Rotations about the C_1-C_2 axis in structures IV and V are −40 and 9°, respectively. (The N atom lies below the plane of the carboxylic acid group in the former case and above it in the latter.) A staggered arrangement of the vicinal N−H and C−H bonds is obtained for structure IV, but the dihedral angles are closer to an eclipsed conformation in structure V. The N lone pair of conventional valence theory is roughly aligned with the $C-H_3$ bond in structure IV; here, the $N-H_5$ bond is oriented toward the hydroxide O. In structure

TABLE 1: B3LYP/6-311G Optimized Geometries**

	isomer				
	I	II	III	IV	V
			Bond[a]		
C_1-C_2	1.525	1.539	1.533	1.520	1.555
C_1-O_1	1.225	1.219	1.223	1.222	1.222
C_1-O_2	1.382	1.386	1.388	1.389	1.362
C_2-N	1.474	1.473	1.474	1.481	1.497
O_2-H_1	0.971	0.967	0.971	0.970	0.997
C_2-H_2	1.091	1.094	1.092	1.104	1.090
C_2-H_3	1.091	1.094	1.091	1.089	1.090
$N-H_4$	1.013	1.014	1.012	1.011	1.010
$N-H_5$	1.013	1.014	1.013	1.011	1.012
			Angle[b]		
$O_1-C_1-O_2$	123.4	120.6	122.9	122.8	124.8
$O_1-C_1-C_2$	126.1	124.1	127.6	126.5	123.6
$O_2-C_1-C_2$	110.5	115.3	110.5	109.6	111.6
C_1-C_2-N	113.2	113.2	116.7	109.7	108.7
$H_1-O_2-C_1$	108.4	110.7	107.8	108.4	103.0
$H_2-C_2-C_1$	108.1	108.6	106.8	106.1	108.6
H_2-C_2-N	110.4	109.6	109.8	115.6	114.2
$H_2-C_2-H_3$	106.4	107.0	106.0	107.4	107.7
$H_3-C_2-C_1$	108.1	108.6	107.0	106.7	107.4
H_3-C_2-N	110.4	109.6	110.0	110.8	110.0
H_4-N-C_2	109.7	109.4	109.8	111.5	113.0
H_5-N-C_2	109.7	109.4	110.0	109.4	112.3
H_5-N-H_4	106.8	106.5	106.8	110.5	109.4
			Dihedral[b]		
$H_1-O_2-C_1-O_1$	0.000	180.0	0.12	−2.97	178.8
$O_2-C_1-C_2-N$	−180.0	−180.0	−3.45	−40.0	8.77
$H_5-N-C_2-H_3$	62.8	63.3	61.6	167.2	−140.0
$H_4-N-C_2-H_2$	−62.8	−63.2	−64.8	52.3	105.6

[a] Distances in angstroms. [b] Angles in degrees.

TABLE 2: MP2/6-311G Optimized Geometries**

	isomer				
	I	II	III	IV	V
			Bond[a]		
C_1-C_2	1.524	1.534	1.528	1.515	1.538
C_1-O_1	1.204	1.197	1.204	1.203	1.200
C_1-O_2	1.354	1.361	1.356	1.355	1.340
C_2-N	1.450	1.449	1.452	1.461	1.470
O_2-H_1	0.969	0.965	0.969	0.969	0.983
C_2-H_2	1.095	1.097	1.094	1.102	1.093
C_2-H_3	1.095	1.097	1.094	1.091	1.093
$N-H_4$	1.016	1.016	1.014	1.014	1.012
$N-H_5$	1.016	1.016	1.014	1.014	1.013
			Angle[b]		
$O_1-C_1-O_2$	123.0	120.5	122.7	122.8	123.8
$O_1-C_1-C_2$	125.4	124.1	124.4	125.3	122.8
$O_2-C_1-C_2$	111.5	115.3	112.9	111.9	113.4
C_1-C_2-N	115.5	115.5	119.1	112.6	111.1
$H_1-O_2-C_1$	106.8	110.3	106.2	106.6	105.0
$H_2-C_2-C_1$	107.6	108.1	106.0	105.5	107.8
H_2-C_2-N	110.0	109.4	109.7	115.0	114.4
$H_2-C_2-H_3$	105.5	105.9	105.3	106.9	106.9
$H_3-C_2-C_1$	107.6	108.1	106.0	106.4	106.4
H_3-C_2-N	110.0	109.4	109.8	109.9	109.9
H_4-N-C_2	109.6	109.3	110.2	109.8	112.3
H_5-N-C_2	109.6	109.3	110.3	110.0	111.7
H_5-N-H_4	105.4	105.3	106.1	107.5	107.8
			Dihedral[b]		
$H_1-O_2-C_1-O_1$	−0.015	180.0	0.054	−1.558	179.1
$O_2-C_1-C_2-N$	180.0	180.0	−1.992	−37.00	11.25
$H_5-N-C_2-H_3$	64.48	64.9	63.55	178.3	−143.1
$H_4-N-C_2-H_2$	−64.47	65.30	−64.28	57.08	−64.80

[a] Distances in angstroms. [b] Angles in degrees.

TABLE 3: Total and Relative Energies

method	isomer	E_{total} (au)	ΔE^a	$\Delta E_{zpe}{}^b$	$\Delta E_{expt}{}^{18}$
B3LYP/6-311G**					
	I	−284.518 091	0.00	0.00	0.00
	II	−284.508 978	5.72	5.50	
	III	−284.515 563	1.59	1.63	
	IV	−284.512 842	3.29	3.28	
	V	−284.517 327	0.48	0.82	1.4 ± 0.43
MP2/6-311G**					
	I	−283.772 784	0.00	0.00	0.00
	II	−283.763 409	5.88	5.62	
	III	−283.770 240	1.60	1.67	
	IV	−283.768 139	2.91	2.94	
	V	−283.771 728	0.66	1.05	1.4 ± 0.43

[a] Total energy differences in kilocalories per mole without zero-point energy correction. [b] Total energy differences in kilocalories per mole with zero-point energy correction.

V, the O−H bond points toward the putative N lone pair, and a slightly longer O−H bond length is found in Tables 1 and 2 for this geometry.

3.2. Energies. The total energies of the five isomers are displayed in Table 3. The B3LYP relative energies are within 0.4 kcal/mol of their MP2 counterparts. Zero-point corrections have little effect on these results. The global minimum predicted by both methods, structure I, is <2 kcal/mol more stable than structures III and V. Our results are in agreement with previous experimental and theoretical studies that conclude that structure I is the most stable isomer and that structure V is the next lowest conformer.[15,17−22] (Coupled-cluster calculations with a double ζ plus polarization basis reverse the order of structures III and V, but the energy difference is only 0.5 kcal/mol.[23]) The relative energies of Table 3 are in very good agreement with the experimental values of Suenram and Lovas.[15]

3.3. Vertical Ionization Energies. The first six vertical ionization energies of each of the glycine isomers are compiled in Table 4 and are compared with experimental results.[3,4] The corresponding Dyson orbitals are plotted in Figures 3−7. In addition to the P3 results which include relaxation and correlation effects, the values based on Koopmans's theorem also are given. Pole strengths for the P3 ionization energies are ~0.9 and therefore validate the perturbative approximations on which the P3 method is based. Discrepancies between the Koopmans and P3 results indicate that relaxation and correlation corrections vary from 1.0 to 1.8 eV and that the predicted order of final states changes in structures III and V as a result.

Two experimental reports on glycine photoelectron spectra have been published.[3,4] In one report, a level diagram is given,[3] and in the other, the spectrum is displayed without numerical data on ionization energies.[4] Approximate values therefore are displayed in Table 4. The spectrum has three bands of comparable intensities in the low binding energy region.[4] A larger feature with three local maxima is found at higher binding energies. In both works, final-state energies are assigned in the same order: $\pi(CO) > a''(n_O) > a'(n_O) > a''(n_N)$. Semiempirical CNDO calculations were performed in conjunction with the experimental work.[4] The authors did not report details of the calculations; a trigonal amino group that is coplanar with the carboxylate atoms may have resulted from the CNDO optimization. Such a result would account for the $a''(n_N)$ description of the highest occupied molecular orbital.

The predicted ionization energies of the most stable isomer, structure I, agree somewhat more closely with estimates based on the spectrum[4] than with those based on the level diagram.[3] For the more clearly resolved trio of low binding energy peaks, the P3 calculations differ from the experimental estimates by

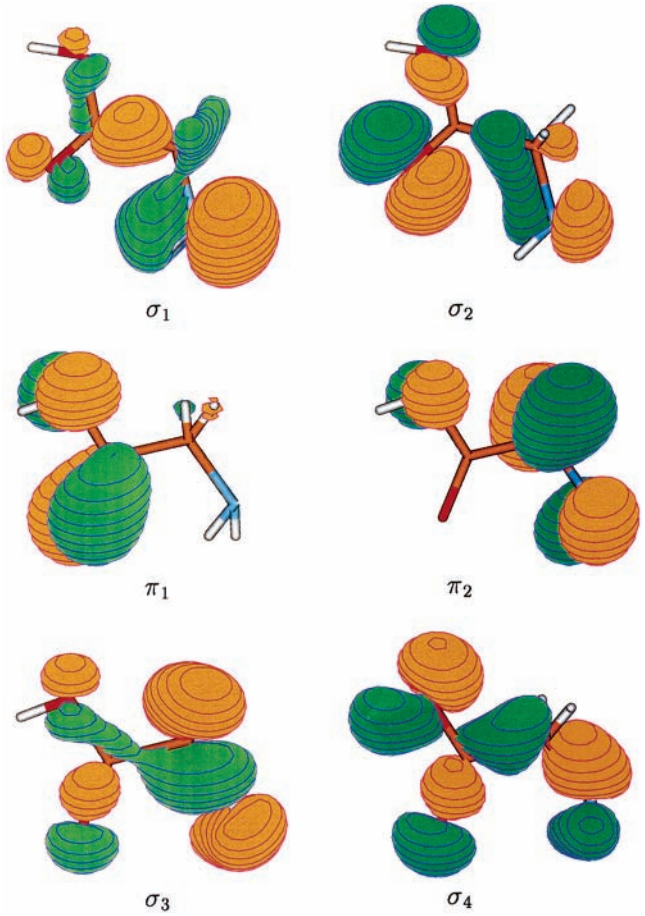

Figure 3. Dyson orbitals for structure I.

TABLE 4: Ionization Energies (eV) and P3 Pole Strengths

isomer	group	orbital	Koopmans	P3	expt[3] (from ref 4)	pole strength
I	C_s	σ_1	11.3	9.9	10.0 (~10)	0.91
		σ_2	12.7	11.0	11.1 (~11.2)	0.90
		π_1	13.3	12.2	12.1 (~12.2)	0.90
		π_2	14.5	13.5	~13.8 (~13.5)	0.92
		σ_3	15.8	14.6	~14.3 (~14.2)	0.91
		σ_4	16.8	14.8	~14.6 (~15.0)	0.91
II	C_s	σ_1	11.4	10.0	10.0 (~10.0)	0.91
		σ_2	12.7	10.9	11.1 (~11.2)	0.90
		π_1	13.2	12.0	12.1 (~12.2)	0.90
		π_2	14.8	13.8	~13.8 (~13.5)	0.92
		σ_3	16.0	14.7	~14.3 (~14.2)	0.91
		σ_4	16.5	14.8	~14.6 (~15.0)	0.90
III	C_s	σ_1	11.0	9.6	10.0 (~10.0)	0.91
		σ_2	13.2	11.4	11.1 (~11.2)	0.90
		π_1	12.7	12.0	12.1 (~12.2)	0.90
		π_2	14.8	13.6	~13.8 (~13.5)	0.92
		σ_3	16.0	14.5	~14.3 (~14.2)	0.91
		σ_4	16.5	14.6	~14.6 (~15.0)	0.91
IV	C_1	σ_1	11.1	9.8	10.0 (~10.0)	0.91
		σ_2	12.5	10.8	11.1 (~11.2)	0.90
		π_1	13.2	12.0	12.1 (~12.2)	0.90
		σ_3	15.0	13.9	~13.8 (~13.5)	0.91
		σ_4	15.8	14.3	~14.3 (~14.2)	0.91
		π_2	16.2	14.7	~14.6 (~15.0)	0.90
V	C_1	σ_1	11.5	10.0	10.0 (~10.0)	0.91
		σ_2	12.8	11.3	11.1 (~11.2)	0.90
		π_1	12.5	11.4	12.1 (~12.2)	0.90
		σ_3	15.2	13.5	~13.8 (~13.5)	0.90
		π_2	15.2	13.9	~14.3 (~14.2)	0.91
		σ_4	16.8	15.2	~14.6 (~15.0)	0.90

0.2 eV or less. In the three remaining cases, agreement with experiment is more difficult to judge because of the uncertainties

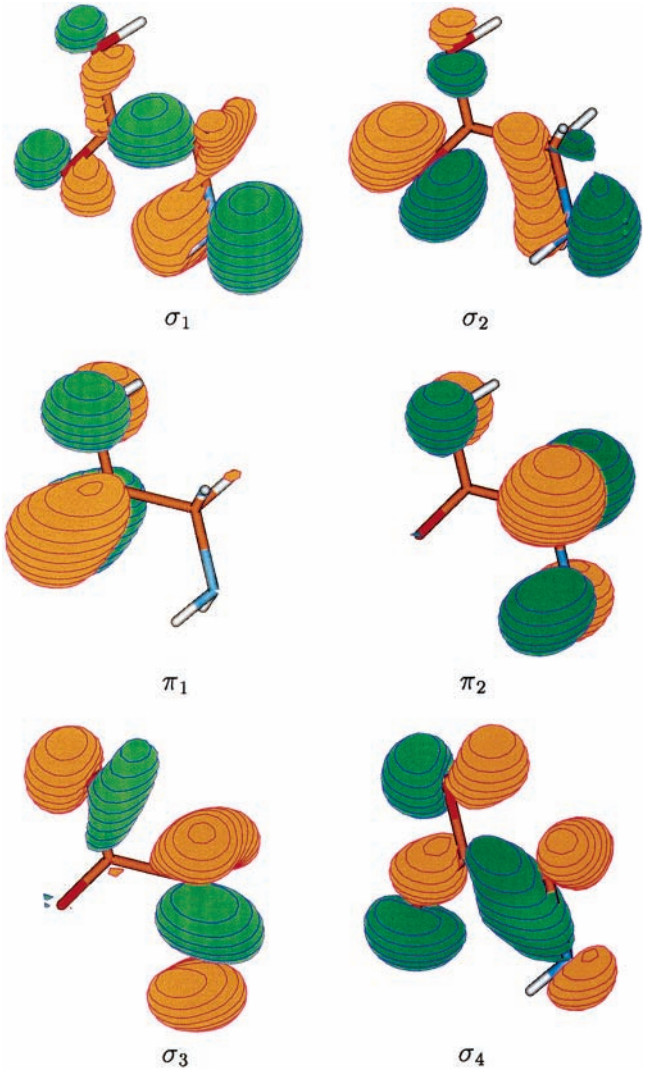

Figure 4. Dyson orbitals for structure II.

of visual estimates based on the published spectrum. Given the small relative energies of structures III and V, it is not possible to ignore the possibility that they also are contributing to the observed peaks. In both of these cases, the order of the second and third final states changes as a result of P3 corrections to Koopmans results. For structure III, the close correspondence with experiment is maintained for the second and third experimental peaks. However, for structure V, the two predicted ionization energies are almost degenerate and coincide with the position of the second observed peak. In all of the C_s structures, the order of final states predicted at the P3 level is the same, with $^2A''$ assignments for the third and fourth ionization energies.

P3 results, especially those pertaining to the lowest ionization energy of each structure, are sufficiently accurate to enable a more reliable evaluation of reactivity descriptors. Important relaxation and correlation corrections to estimates based on Koopmans's theorem may be determined efficiently with this method.

3.4. Dyson Orbitals. The order of final states given in Table 4 is not in agreement with that given in the experimental reports. Even in the event of agreement in this respect, assignments based on the C_s and C_1 point groups alone convey little information about the differences in electronic structure associated with each of the ionization energies. Therefore, Dyson orbitals for each of the structures are discussed here in terms of the amplitudes displayed in Figures 3−7.

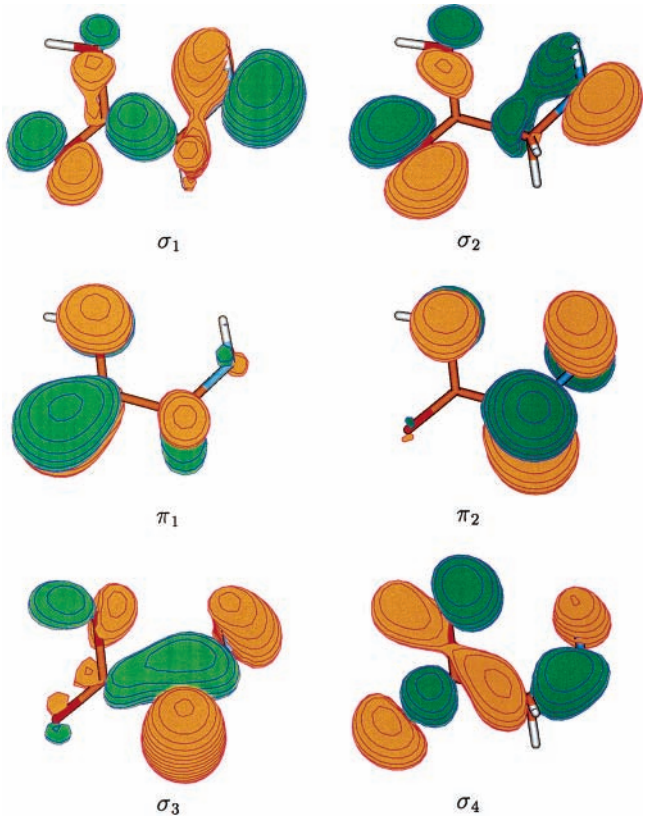

Figure 5. Dyson orbitals for structure III.

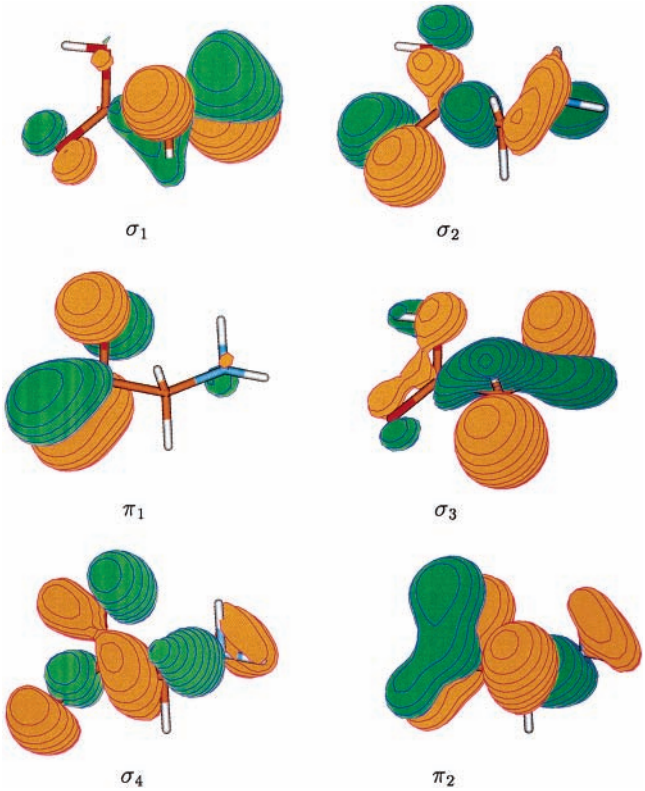

Figure 6. Dyson orbitals for structure IV.

3.4.1. Structure I. In the Dyson orbital (Figure 3) of the lowest ionization energy, σ_1, the largest contributions are made by N functions such that the largest lobes resemble those of the ammonia molecule's highest occupied molecular orbital. This lone-pair feature is accompanied by smaller contributions on other nuclei. The second Dyson orbital's largest component is

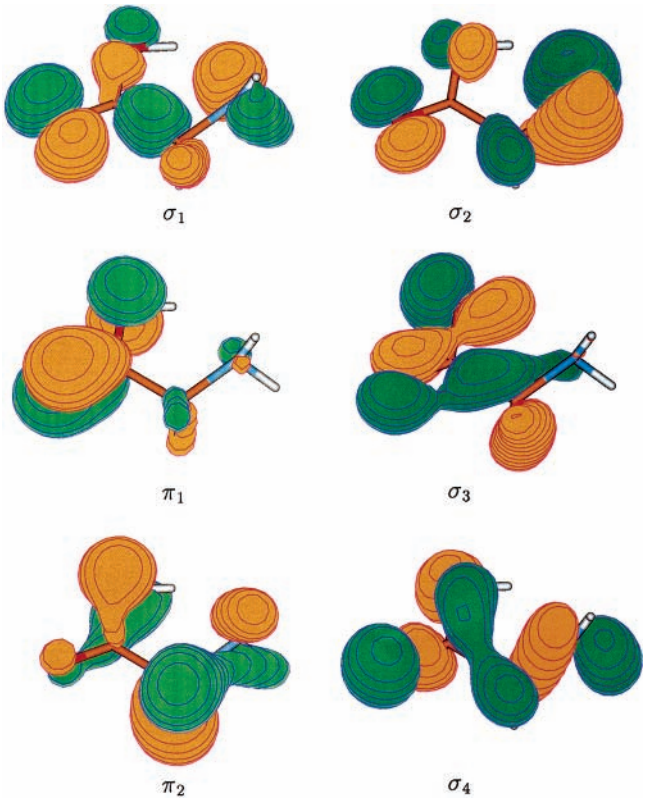

Figure 7. Dyson orbitals for structure V.

a 2p function on O_1 that is parallel to the symmetry plane. Antibonding relationships in this orbital, σ_2, occur between the O_1 2p function and 2p functions on N and O_2. A C_1-C_2 bonding lobe also can be discerned in this orbital. Destructive interference in the third Dyson orbital, π_1, results in a π node between the carbonyl group and the hydroxide O.

C−H and N−H bonding lobes with alternating phases and a smaller contribution from a 2p orbital on O_2 predominate in the fourth Dyson orbital, π_2. Between the amino, methylene, and hydroxide regions lie π nodes. Similar C−H and N−H bonding lobes with positive phase relationships across the symmetry plane are found in the fifth Dyson orbital, σ_3. Some delocalization into O_1 and O_2 2p functions also can be seen. A series of nodes are interleaved between O 2p functions and C_1-C_2 and C_2-N bonding lobes in the Dyson orbital for the sixth ionization energy, σ_4.

3.4.2. Structure II. For the least stable of the minima, the O_2-H_1 bond is rotated away from the carbonyl O. The resulting loss of Coulombic stabilization from the O_2-H_1 interaction has little effect on the first four Dyson orbitals. (Compare Figures 3 and 4.) In the fifth and sixth Dyson orbitals, contributing O 2p functions are rotated. For the σ_3 case, the carbonyl O contribution nearly vanishes for the same value of the orbital contour.

The small changes in the ionization energies relative to the values of structure I may be explained in terms of the altered electrostatic environment caused by the relocation of the hydroxide's proton, H_1. When the distance between the most prominent lobes and H_1 is decreased in structure II, the ionization energy is larger. Therefore, the first ionization energy changes from 9.9 eV in structure I to 10.0 eV in structure II. The same effect is seen for the fourth and fifth Dyson orbitals. For the second and third Dyson orbitals, the opposite trend is realized. In the third and fourth cases, the largest changes take place and are associated with the large lobes on the carbonyl O and the C_2-H bonds, respectively. There is a cancellation of destabilizing and stabilizing effects in the sixth Dyson orbital.

3.4.3. Structure III. Rotation of the amino group away from the carbonyl O and toward the hydroxide O results in significant changes in the ionization energies which may be explained by comparisons between Figures 3 and 5. Component lobes in the Dyson orbitals of the lowest ionization energy for structures I and III are approximately the same. Aside from the displacement of the amino group's contributions, the most notable change occurs in the size of the carbonyl O 2p lobes. The amino lobes are closer to the more negatively charged O in structure III. In addition, functions on the amino group have a bonding relationship with an O_1 2p function in structure I that is replaced by an antibonding relationship with an O_2 2p function in structure III. Therefore, the ionization energy is reduced by 0.3 eV in the less stable isomer. In the second Dyson orbital, the lobe on the amino group that is delocalized into the C_1-C_2 bonding region has an antibonding relationship with the carbonyl O in structure I; rotation of the amino group weakens this interaction. The second ionization energy is larger in structure III by 0.4 eV as a result. Because methylene C−H bonds are closer to the carbonyl group in structure III than in structure I, hyperconjugative destabilization is accentuated in the π_1 Dyson orbital of Figure 5. The third ionization energy shifts from 12.2 to 12.0 eV as a result.

Changes in π interactions in the Dyson orbitals have a smaller, but opposite, effect on the fourth ionization energy. The in-phase relationship between the hydroxide O 2p orbital and N−H lobes in structure III is activated by the rotation of the amino group. Many subtle changes take place in the Dyson orbitals of the fifth ionization energy between Figures 3 and 5. In the sixth Dyson orbital, the same pattern of lobes and nodes survives the rotation of the amino group. In these two cases, several competing factors lead to lower ionization energies in structure III.

3.4.4. Structure IV. Despite the lower point group of this isomer, comparisons with structure I are made possible by examining Figures 3 and 6. Whereas the amino group rotation preserved C_s symmetry in the previous structure, here the point group is C_1. The Dyson orbital of the first ionization energy is similarly constituted in structures I and IV. In the latter case, amino-centered lobes are closer to the negatively charged hydroxide O and a weak bonding interaction between these lobes and the carbonyl O 2p contribution is deactivated. Therefore, the first ionization energy is slightly lower for structure IV than for structure I. Dyson orbitals for the second ionization energy have large amplitudes around the carbonyl O in both isomers. Positively charged hydrogens in the amino group are more distant from the carbonyl O in structure IV, and the ionization energy decreases accordingly. For similar reasons, the ionization energy also decreases for the third final state, for the largest amplitudes remain concentrated on the carbonyl O in structures I and IV.

The π antibonding destabilization of the C−H lobes by the 2p orbital on the hydroxide O that occurs in the fourth Dyson orbital of structure I no longer applies in structure IV, leading to a larger ionization energy in the latter isomer. The fifth Dyson orbital of structure IV bears a close resemblance to the sixth Dyson orbital of structure I. There is a weaker resemblance between the sixth Dyson orbital of structure IV and the fifth Dyson orbital of structure I. This crossing may involve deeper levels, for the emergence of a carboxylate π contribution is clearly visible for the sixth Dyson orbital of Figure 6.

3.4.5. Structure V. In the second most stable isomer, structure V, a qualitative change takes place in the amplitudes of the first two Dyson orbitals. Closer proximity between the amino N and the hydroxide H and a larger distance between the amino protons and the carbonyl O produce a switching in the character of these two orbitals. Now the first Dyson orbital's largest lobes occur on the carbonyl O, and N 2p contributions are most prominent in the second Dyson orbital. There is less localization on the dominant group in structure V for both orbitals. The appearance of the third Dyson orbital remains approximately the same. Given the similar orientation of the hydroxide groups in structures V and II, the best way to evaluate the effect of amino group rotation is to compare the ionization energies of these isomers. A smaller value is obtained for isomer V because of the larger distance between the positively charged amino H atoms and the carbonyl O.

The Dyson orbitals of the three remaining ionization energies are not easily related to their counterparts in other structures. There is a resemblance between the nodal patterns of the fourth Dyson orbital of Figure 7 and the sixth Dyson orbital of isomer II. Shifts in ionization energies are the products of many competing factors.

4. Conclusions

Five isomers of glycine corresponding to minima in B3LYP and MP2 geometry optimizations lie within 6 kcal/mol of each other. The two most stable structures, I and V, are practically isoenergetic and a third structure, III, may be present in gas-phase samples that are prepared by typical jet-cooling techniques. Structures I and III have C_s symmetry, but structure V has C_1 symmetry. No definitive ordering of these three isomers is possible on the basis of calculations.

Calculations have shown that the vertical ionization energies of glycine vary with conformation, but the resolution of published spectra does not suffice to reach conclusions on which structures are most stable. The P3 results are in agreement with peak values reported in experiments that are approximately 30 years old.[3,4] Experiments performed with higher resolution may be able to discern greater compatibility with the predictions for isomer I when sample temperatures are low. Should such data become available, more precise calculations may be needed.

P3 calculations facilitate the evaluation of reactivity parameters such as the chemical potential and molecular hardness with a higher degree of confidence. For isomers I−IV, the Dyson orbitals for the first ionization energy display large amplitudes on the amino group and bear some resemblance to the highest occupied molecular orbital of ammonia. For the second ionization energy, the largest contributions to the corresponding Dyson orbitals are made by 2p functions on the carbonyl O that are perpendicular to the C_1-O_2 axis and parallel to the carboxylate group's nuclear plane. In structure V, there is enhanced mixing of these N and O contributions. Lone-pair character on N or O is present in every structure for the first two Dyson orbitals. In all structures, the third Dyson orbital is a π function distributed over the carbonyl region and the hydroxide O, with a node in between. Conformational isomerization leads to shifts in these ionization energies which may be explained in terms of Coulombic interactions and changes in phase relationships. C−H bonding lobes are most prominent in the fourth Dyson orbital of the C_s structures, which has a'' symmetry. Dyson orbitals for the higher ionization energies consist of σ lobes with many interleaving nodes.

Acknowledgment. Support for this research was provided by FONDECYT through project 1020534 (A.T.-L.), by a CONICYT 2002 Doctoral Thesis Support Scholarship (Beca de Apoyo a la Tesis doctoral 2002) to B.H., who is a CONICYT fellow, and by the National Science Foundation through grant CHE-0135823 to Kansas State University.

References and Notes

(1) Examples include CHARMM (www.charmm.org), AMBER (amber.scripps.edu), and GROMOS (www.igc.ethz.ch/gromos).

(2) Ground-state cations of glycine in the gas phase and their fragmentation patterns were examined with correlated, ab initio methods in Simón, S.; Sodupe, M.; Bertrán, J. *J. Phys. Chem. A* **2002**, *106*, 5697. Diffuse-bound anions based on zwitterionic and neutral structures of glycine were considered in Gutowski, M.; Skurski, P.; Simons, J. *J. Am. Chem. Soc.* **2000**, *122*, 10159.

(3) Debies, T. P.; Rabalais, J. W. *J. Electron. Spectrosc. Relat. Phenom.* **1974**, *3*, 315.

(4) Klasinc, L. *J. Electron. Spectrosc. Relat. Phenom.* **1976**, *8*, 161.

(5) Powis, I.; Rennie, E. E.; Hergenhahn, U.; Kugeler, O.; Bussy-Socrate, R. *J. Phys. Chem. A* **2003**, *107*, 25.

(6) Ortiz, J. V. In *Computational Chemistry: Reviews of Current Trends*; Leszczynski, J., Ed.; World Scientific: Singapore, 1997; Vol. 2, p 1.

(7) Ortiz, J. V. *Adv. Quantum Chem.* **1999**, *35*, 33.

(8) Frisch, M. J.; Trucks, G. W.; Schlegel, H. B.; Scuseria, G. E.; Robb, M. A.; Cheeseman, J. R.; Zakrzewski, V. G.; Montgomery, J. A., Jr.; Stratmann, R. E.; Burant, J. C.; Dapprich, S.; Millam, J. M.; Daniels, A. D.; Kudin, K. N.; Strain, M. C.; Farkas, O.; Tomasi, J.; Barone, V.; Cossi, M.; Cammi, R.; Mennucci, B.; Pomelli, C.; Adamo, C.; Clifford, S.; Ochterski, J.; Petersson, G. A.; Ayala, P. Y.; Cui, Q.; Morokuma, K.; Malick, D. K.; Rabuck, A. D.; Raghavachari, K.; Foresman, J. B.; Cioslowski, J.; Ortiz, J. V.; Baboul, A. G.; Stefanov, B. B.; Liu, G.; Liashenko, A.; Piskorz, P.; Komaromi, I.; Gomperts, R.; Martin, R. L.; Fox, D. J.; Keith, T.; Al-Laham, M. A.; Peng, C. Y.; Nanayakkara, A.; Gonzalez, C.; Challacombe, M.; Gill, P. M. W.; Johnson, B.; Chen, W.; Wong, M. W.; Andres, J. L.; Gonzalez, C.; Head-Gordon, M.; Replogle, E. S.; Pople, J. A. *Gaussian 98*, revision A.7; Gaussian, Inc.: Pittsburgh, PA, 1998.

(9) Frisch, M. J.; Trucks, G. W.; Schlegel, H. B.; Scuseria, G. E.; Robb, M. A.; Cheeseman, J. R.; Zakrzewski, V. G.; Montgomery, J. A., Jr.; Stratmann, R. E.; Burant, J. C.; Dapprich, S.; Millam, J. M.; Daniels, A. D.; Kudin, K. N.; Strain, M. C.; Farkas, O.; Tomasi, J.; Barone, V.; Mennucci, B.; Cossi, M.; Adamo, C.; Jarmillo, J.; Cammi, R.; Pomelli, C.; Ochterski, J.; Petersson, G. A.; Ayala, P. Y.; Morokuma, K.; Malick, D. K.; Rabuck, A. D.; Raghavachari, K.; Foresman, J. B.; Ortiz, J. V.; Cui, Q.; Baboul, A. G.; Clifford, S.; Cioslowski, J.; Stefanov, B. B.; Liu, G.; Liashenko, A.; Piskorz, P.; Komaromi, I.; Gomperts, R.; Martin, R. L.; Fox, D. J.; Keith, T.; Al-Laham, M. A.; Peng, C. Y.; Nanayakkara, A.; Challacombe, M.; Gill, P. M. W.; Johnson, B.; Chen, W.; Wong, M. W.; Andres, J. L.; Gonzalez, C.; Head-Gordon, M.; Replogle, E. S.; Pople, J. A. *Gaussian 99*, development version (revision B.06+); Gaussian, Inc.: Pittsburgh, PA, 1998.

(10) (a) Becke, A. D. *J. Chem. Phys.* **1993**, *98*, 5648. (b) Lee, C.; Yang, W.; Parr, R. G. *Phys. Rev. B* **1988**, *37*, 785. (c) Mielich, B.; Savin, A.; Stoll, H.; Preuss, H. *Chem. Phys. Lett.* **1989**, *157*, 200.

(11) (a) Krishnan, R.; Binkley, J. S.; Seeger, R.; Pople, J. A. *J. Chem. Phys.* **1980**, *72*, 650. (b) Frisch, M. J.; Pople, J. A.; Binkley, J. S. *J. Chem. Phys.* **1984**, *80*, 3265.

(12) Ortiz, J. V. *J. Chem. Phys.* **1996**, *104*, 7599.

(13) Ferreira, A. M.; Seabra, G.; Dolgounitcheva, O.; Zakrzewski, V. G.; Ortiz, J. V. In *Quantum-Mechanical Prediction of Thermochemical Data*; Cioslowski, J., Ed.; Kluwer: Dordrecht, The Netherlands, 2001; p 131.

(14) Schaftenaar, V. *MOLDEN*; CAOS/CAMM Center: The Netherlands, 1991.

(15) Suenram, R. D.; Lovas, F. J. *J. Mol. Spectrosc.* **1978**, *72*, 372.

(16) Locke, M. J.; McIver, R. T. *J. Am. Chem. Soc.* **1983**, *105*, 4226.

(17) Schaffer, V.; Sellers, H. L.; Lovas, F. G.; Suenram, R. D. *J. Am. Chem. Soc.* **1980**, *102*, 6566.

(18) Suenram, R. D.; Lovas, F. J. *J. Am. Chem. Soc.* **1980**, *102*, 7180.

(19) Jensen, F. *J. Am. Chem. Soc.* **1992**, *114*, 9533.

(20) Ai, H.; Bu, Y.; Han, K. *J. Chem. Phys.* **2002**, *117*, 7593.

(21) Jensen, J. H.; Gordon, M. S. *J. Am. Chem. Soc.* **1991**, *113*, 7917.

(22) Császár, A. G. *J. Am. Chem. Soc.* **1992**, *114*, 9568.

(23) Hu, C.-H.; Shen, M.; Schaefer, H. F. *J. Am. Chem. Soc.* **1993**, *115*, 2923.